

Cytoplasmic streaming in *Drosophila* oocytes varies with kinesin activity and correlates with the microtubule cytoskeleton architecture

Sujoy Ganguly^{a,1}, Lucy S. Williams^{b,1}, Isabel M. Palacios^{b,2,3}, and Raymond E. Goldstein^{a,2,3}

^aDepartment of Applied Mathematics and Theoretical Physics, University of Cambridge, Wilberforce Road, Cambridge CB3 0WA, United Kingdom; and ^bDepartment of Zoology, University of Cambridge, Downing Street, Cambridge CB2 3EJ, United Kingdom

Edited by Harry L. Swinney, University of Texas at Austin, Austin, TX, and approved July 30, 2012 (received for review March 23, 2012)

Cells can localize molecules asymmetrically through the combined action of cytoplasmic streaming, which circulates their fluid contents, and specific anchoring mechanisms. Streaming also contributes to the distribution of nutrients and organelles such as chloroplasts in plants, the asymmetric position of the meiotic spindle in mammalian embryos, and the developmental potential of the zygote, yet little is known quantitatively about the relationship between streaming and the motor activity which drives it. Here we use Particle Image Velocimetry to quantify the statistical properties of Kinesin-dependent streaming during mid-oogenesis in *Drosophila*. We find that streaming can be used to detect subtle changes in Kinesin activity and that the flows reflect the architecture of the microtubule cytoskeleton. Furthermore, based on characterization of the rheology of the cytoplasm *in vivo*, we establish estimates of the number of Kinesins required to drive the observed streaming. Using this *in vivo* data as the basis of a model for transport, we suggest that the disordered character of transport at mid-oogenesis, as revealed by streaming, is an important component of the localization dynamics of the body plan determinant *oskar* mRNA.

cytoplasmic viscosity | fluid dynamics | random transport | cellular asymmetries

Motor proteins of the kinesin, myosin and dynein families transport molecules, organelles, and membrane vesicles along the cytoskeleton in order to organize cellular components for proper cell function. A striking example of motor dependent organization takes place when the microtubule (MT) cytoskeleton of the *Drosophila melanogaster* oocyte is reorganized at mid-oogenesis to direct the asymmetric localization of the body-plan determinants *bicoid*, *oskar*, and *gurken* mRNAs (1). The polarized MT cytoskeleton, as well as Dynein and Kinesin-1, are required for positioning of the oocyte nucleus to a point at the anterior margin, defining the dorsal-ventral (DV) axis of the embryo by directing the accumulation and local translation of *gurken* mRNA to one side of the nucleus. Microtubules, Dynein, and Kinesin-1 are also essential for localization of *bicoid* and *oskar* mRNAs to the anterior (A) and posterior (P) poles of the oocyte, respectively, an essential step in determination of the AP axis of the embryo (1). At these stages of mid-oogenesis, the oocyte is roughly hemispherical, extending approximately 100 μm along the AP axis. (Fig. 1A). The MTs are nucleated from the anterolateral cortex in a gradient of diminishing abundance toward the posterior pole, where nucleation is absent. The anterior MT network is a dense mesh throughout the cytoplasm. This mesh extends into the extreme posterior, where the MTs are much less abundant (2) (Fig. 1B).

As these developmental determinants are being localized, the MT cytoskeleton and Kinesin-1 also induce bulk movement of the oocyte cytoplasm, known as cytoplasmic streaming (3–7). In late oogenesis, the mRNA encoding the posterior determinant *nanos* is distributed within the ooplasm by this microtubule-dependent flow and anchored at the posterior in an actin-dependent manner

(8). Discovered nearly 240 years ago in plants (9), cytoplasmic streaming occurs in a wide variety of eukaryotic cells, across a range of sizes and developmental stages. Although in all cases it is thought that flows are generated by the cytoskeleton-dependent action of motor proteins—kinesins translocating along microtubules or myosins moving on actin (10)—the precise biological significance of streaming flows has been unclear (11). Potential roles include distribution of nutrients in plants (12, 13), where it has been suggested (14–16) that flows may contribute to mixing of cellular material in a way that would facilitate homeostasis (17), establishing the scale of the *bicoid* gradient in *Drosophila* embryos (18), asymmetric localization of the meiotic spindle in mammalian embryos (19), and development of the zygote (20). Yet, the relationship between the underlying motor activity and the observed flows is poorly understood. Even in the highly regular geometries of plants (e.g., *Chara corallina*), and despite longstanding interest in the nature of cargo transported by the motors and the fluid mechanics of the cytoplasm itself (21, 22), this connection remains an active area of investigation (23, 24). In no system has there been a systematic study connecting motor activity to the induced streaming.

Here we examine the connection between motor activity and cytoplasmic streaming by using Particle Image Velocimetry (PIV) to quantify the Kinesin-1-dependent streaming in the *Drosophila* oocyte at mid-oogenesis. Previous work on this system has focused on particle tracking and maximum intensity projections to quantify the streaming speed (3–7). Though these methods determine the presence of flows and give some estimates of typical speeds, much of the spatial information is lost. PIV is a widely used technique in fluid mechanics that analyzes successive images of passive tracers and outputs the entire velocity field (25, 26), and it has been used to characterize microscale biological flows (27).

With the wealth of data that results from PIV (up to 2 million vectors per oocyte) detailed measures of streaming can be obtained. Such measurements allow one to resolve subtle differences between mutants, revealing a quantitative relation between motor activity and flow. We combine these measurements with an *in vivo* rheological study of the oocyte cytoplasm, which allows estimates of the power dissipated by the flows and hence the minimum number of motors needed to drive cytoplasmic

Author contributions: S.G., L.S.W., I.M.P., and R.E.G. designed research, performed research, analyzed data, and wrote the paper.

The authors declare no conflict of interest.

This article is a PNAS Direct Submission.

Freely available online through the PNAS open access option.

¹S.G. and L.S.W. contributed equally to this work.

²I.M.P. and R.E.G. contributed equally to this work.

³To whom correspondence may be addressed. E-mail: R.E.Goldstein@damtp.cam.ac.uk or mip22@cam.ac.uk.

This article contains supporting information online at www.pnas.org/lookup/suppl/doi:10.1073/pnas.1203575109/-DCSupplemental.

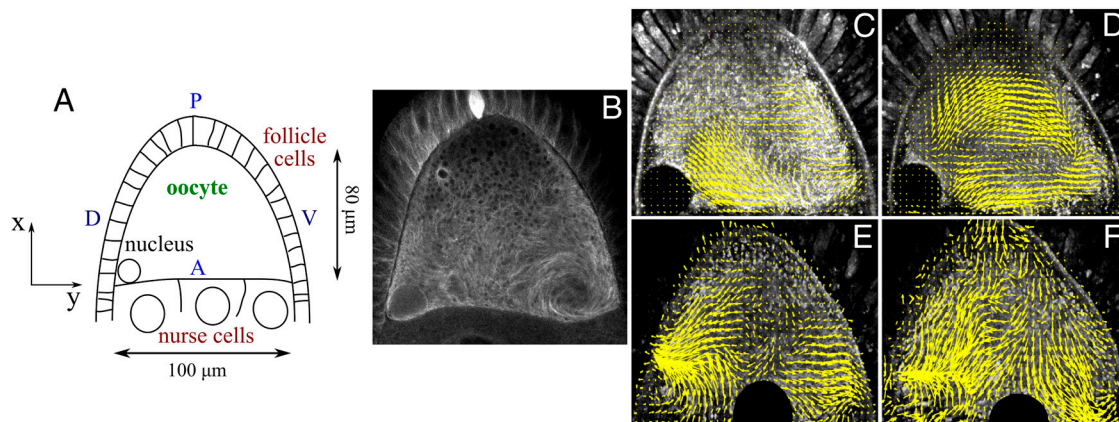


Fig. 1. The *Drosophila* oocyte and PIV analysis of cytoplasmic streaming. (A) Schematic of the oocyte, indicating anterior A, posterior P, dorsal D and ventral V regions, and coordinate system used in text. (B) Live image of dense mesh of microtubules in oocyte with GFP-labelled Jupiter. Flow fields (yellow vectors) for two different oocytes (C–D & E–F) at two different times. The PIV fields are overlaid on images of the autofluorescent particles (white patterns) used as passive tracers of the cytoplasmic streaming. The resulting swirls reflect the projection of 10 frames. Circular black region within each oocyte is the nucleus, approximately 15 μm in diameter.

streaming, in a manner analogous to recent work in plants (23). These measurements also lead to predictions of changes in motor activity or motor number due to mutations in Kinesin-1. Using a statistical analysis of the flow topology and the MT directional correlation function, we find a striking similarity between the long-range correlations in cytoplasmic streaming and those of the underlying MT network. Along with observed correlations between the local average streaming speed and the MT concentration, these results should help benchmark detailed microscopic models connecting motor activity and the architecture of the MT network. This finding inspires a quantitative model of Kinesin mediated mRNA transport in the oocyte, and an analysis of the model parameter space leads us to suggest that long-ranged correlations can significantly enhance transport of *oskar* mRNA in the oocyte.

Results and Discussion

Whereas previous studies of streaming in *Drosophila* (3, 5–7) revealed only a schematic picture of flows, PIV outputs a complete two-dimensional cross-section. Because the oocytes are not always in the same orientation the ensemble of slices represents a number of different rotations about the AP axis. The flows (Fig. 1C–F; **Movies S1** and **S2**) consist of swirls that vary in time within one oocyte and from one to the next. In light of this variability two useful measures of streaming are (i) the probability distribution function (pdf) of fluid speeds and (ii) a statistical description of the geometry of flow patterns.

To test the hypothesis that PIV can resolve subtle changes in motor activity, we analyzed flows in mutants known to reduce Kinesin motility, under the assumption that a reduction in Kinesin heavy chain (Khc) speed would be reflected in the streaming speed. We determined the speed pdf in wild type (WT) oocytes and those lacking Pat1, a protein required for Khc to maximize its motility (28). These distributions (Fig. 2A) have clear peaks and long tails; the latter may reflect a combination of an underlying distribution of motor speeds and the complex three-dimensional MT network geometry. The most important characteristic of these pdfs is the mean speed \bar{v} ; in WT oocytes we find $\bar{v}_{wt} = 21.5 \pm 0.8$ nm/s, while in *pat1* mutants $\bar{v}_{pat1} = 18.3 \pm 1.1$ nm/s. The decrease in the streaming speed in the mutant oocytes is remarkably close to the 20% reduction in Khc speed found by direct measurement of motor motion in extracts of *pat1* mutant cytoplasm (28). Because Kinesin light chain (Klc) and Pat1 (a Klc-like protein) have redundant functions during oogenesis (28), we also analyzed streaming in *klc* mutants, and found that the speed pdfs of *pat1* and *klc* are strikingly similar (Fig. 2A). These findings

demonstrate that PIV provides a quantitative “readout” that is sensitive to molecular details of Kinesin activity. This result also supports the conjecture that the Klc enhances Khc motility. A test of the similarity of the speed pdfs is obtained by rescaling the speed v by its peak value v^* for each distribution, and multiplying the probability by v^* to preserve normalization. As shown in Fig. 2B the three distributions share a common structure, including an approximate power-law tail.

To test the relationship between the local speed of streaming and the concentration of the MT cytoskeleton, we analyzed flows

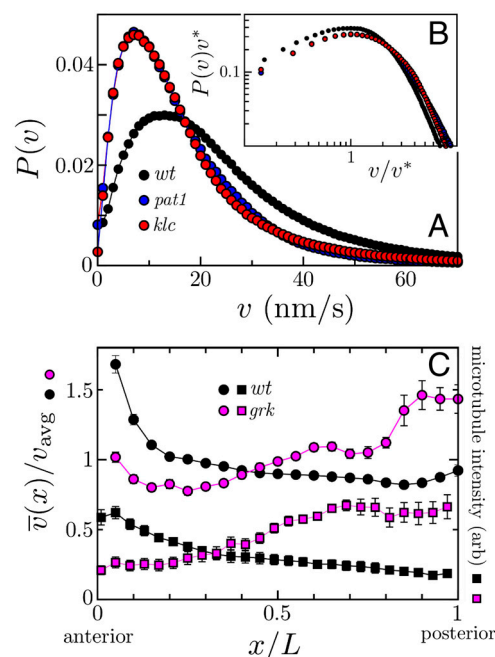


Fig. 2. Statistical measures of streaming. (A) Probability distribution functions of streaming speed in WT oocytes (black, $n = 21$), and oocytes mutant for *kinesin light chain* (*klc* red, $n = 7$) and *pat1* (blue, $n = 12$). The peaks of distributions are 13.2 nm/s (WT) and 8.5 nm/s for *klc* and *pat1* mutants. Mean speeds are 21.5 nm/s (WT), 16.1 nm/s for *klc* mutants and 18.3 nm/s for *pat1* mutants. (B) Log-log plot of speed pdfs scaled by peak velocity v^* of each, showing similar functional forms. (C) Dorsal-ventral-averaged speed scaled by global mean speed [WT: $n = 21$; *gurken* (*grk*): $n = 6$], and MT image intensity [WT: $n = 8$, *gurken* (*grk*): $n = 10$] along the AP axis. Comparison between wild type and *gurken* mutant oocytes indicates reversal of the speed distribution and the MT concentration.

in *gurken* mutants (29, 30). Oocytes lacking Gurken have disrupted cytoskeleton organization, leading to a ‘reverse’ polarity of MTs; the MT network in *gurken* mutant oocytes shows an increased concentration at the posterior, opposite to the WT. We have quantified this reversal by determining the mean streaming speed (averaged over the DV direction) as a function of distance x along the AP axis, and comparing to MT concentration profiles calculated analogously to the speed profiles from tubulin stainings. As shown in Fig. 2C *gurken* mutants display the highest flow speeds and MT network concentration at the posterior, with a reducing gradient towards the anterior. This profile is in contrast with the anterior to posterior gradient seen in WT. This result shows that the typical streaming speed correlates with the MT network concentration.

Because flows in the oocyte are MT-dependent and correlate with MT concentration, we ask how the patterns of swirls relates to the architecture of the MT network. Furthermore, as the speed pdfs are ensemble averages they indicate that no particular rotation about the AP axis is distinguished. A statistically robust quantity with which to obtain the swirl size is the correlation function $C(\mathbf{r})$,

$$C(\mathbf{r}) = \frac{\langle \mathbf{u}(\mathbf{x} + \mathbf{r}) \cdot \mathbf{u}(\mathbf{x}) \rangle - \langle \mathbf{u}(\mathbf{x}) \rangle^2}{\langle \mathbf{u}(\mathbf{x})^2 \rangle - \langle \mathbf{u}(\mathbf{x}) \rangle^2}, \quad [1]$$

where $\mathbf{u}(\mathbf{x})$ is the velocity at \mathbf{x} , and the angular brackets denote averages over all points \mathbf{x} . (As the oocyte is a closed system the three-dimensional average of \mathbf{u} vanishes by incompressibility, but this constraint does not necessarily hold for any two-dimensional slice. In practice, the two-dimensional mean velocity is very small.) When $C(r)$ is 1 or -1 vectors a distance r apart are, on average, parallel or antiparallel, respectively. For these kinds of disordered, swirly flows the distance $|\mathbf{r}| = r_0$ at which $C(\mathbf{r})$ crosses zero defines the typical size of flow features (31). In WT oocytes $r_0 \sim 18 \mu\text{m}$ (Fig. 3A), roughly 20% of the oocyte length at mid-oogenesis. The flow correlation functions of *pat1* and *klc* mutants do not vary significantly from that of the WT,

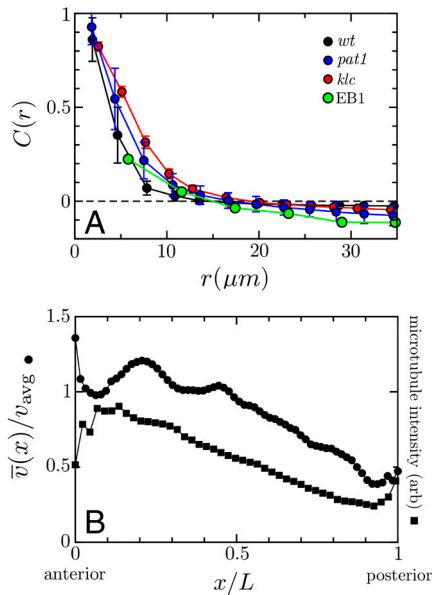


Fig. 3. Statistical measures extracted from the PIV data. (A) Correlation functions as calculated from equation 1 for EB1 microtubule fields (green) and streaming fields in wild type oocytes (black) and oocytes mutant for *pat1* (blue) and *klc* (red). (B) Simultaneous measurements of the average microtubule concentration and mean streaming speed as a function of position along the anterior-posterior cortex. MTs are labelled by JupiterGFP ($n = 1$). A global spatial average correlation over 10 oocytes gives a value of 0.68 ± 0.06 . TauGFP shows a comparable behavior.

indicating that reduced Khc activity does not affect streaming topology (Fig. 3A).

The presence of flow correlations on a scale larger than the network mesh size (submicron) yet smaller than the oocyte size suggests that the MT cytoskeleton should have similar orientational correlations. To test this hypothesis we calculated the MT directional correlation function, defined analogously to Eq. 1, from data obtained by tracking EB1, a protein that labels growing microtubule plus ends (data analyzed with ParticleStats) (2). This cytoskeleton correlation (Fig. 3A) is statistically equivalent to the flow correlation, implying that flow features may be representative of network architecture.

We next analyzed overlaying maps of the vector fields from PIV and from two microtubule binding proteins, Tau and Jupiter (see Movie S2). TauGFP reveals the same MT organization at all stages of oogenesis that has previously been described in fixed preparation (32) and JupiterGFP is a MT-associated protein whose behavior has been shown to accurately reflect MT behavior (33). These *simultaneous* measurements of streaming speed and MT concentration show a very strong correlation (Fig. 3B). A global spatial average correlation over all oocytes gives a value of 0.68 ± 0.06 ($n = 10$).

The fact that flows are abolished when Kinesin is mutated, and slower when Khc is slower, suggests that Kinesin drags objects large enough to drive flow of the entire cytosol, and it does so with respect to the MT network. Streaming then has an impact on the distribution of the MTs, as suggested by the movement of MTs seen in time lapse movies of Jupiter GFP (Movie S2), although the precise nature of the impact is not yet understood. It is possible that flows have also an impact on motor-dependent transport. As streaming occurs at low Reynolds number (34) and is Khc-dependent [there is no observable streaming in *khc* mutants (6)] the work done by Kinesin motion on the cytoplasm is dissipated by viscous mechanisms. The rate of dissipation P_s can be expressed as $P_s = N_m \phi_m$, where N_m is the number of motors contributing to streaming, and ϕ_m is the power of a motor. If we use for Khc a representative value of the force/step of 5.5 pN (35) and an average speed in the cytoplasm of 115 nm/s (in vivo measurement, $n = 50$), then $\phi_m \approx 630 \times 10^{-21} W$. Adopting thermal energy $k_B T$ as a convenient unit of measure, where k_B is Boltzmann’s constant and T is the absolute temperature, this motor power can be reexpressed as $\phi_m \sim 150 k_B T/s$.

Any measure of power dissipation in a viscous fluid depends on gradients in the flow (the shear rate). Because PIV yields the velocity field averaged over a spatial grid ($3 \times 3 \mu\text{m}$), it is not possible to measure directly gradients on smaller scales, but given that cytoplasm moves through a meshwork of microtubules as flow in a ‘porous medium’, we deduce that the mesh size defines the smallest scale of gradients. Direct visualization of MTs (2) indicates a mesh scale of 0.1–0.3 μm , so the maximum shear rate possible is $\mathcal{O}(1) s^{-1}$.

To relate dissipation to the flow we need the cytoplasm rheology, the relationship between the forces and fluid velocities. The simplest behavior is a Newtonian fluid, with proportionality between the two, but as the cytoplasm is densely packed with polymers it is likely to exhibit non-Newtonian behavior such as a frequency-dependent viscosity (36). We measured the viscosity using Single Point Passive Microrheology (37–39) in quiescent *khc*²⁷ mutant oocytes (6), using several bead sizes and coatings (see SI Text). The frequency-dependent viscosity in Fig. 4 indicates that even at the largest possible shear rates seen by PIV the cytoplasm is Newtonian, with a viscosity $\mu = 1.38 \text{ Pa}\cdot\text{s}$ similar to glycerol. There is non-Newtonian behavior on timescales shorter than approximately 0.4 s, which is likely due to elastic relaxation of the MT and/or actin networks (see SI Text). At the instantaneous velocity of Kinesin during a step, modest non-Newtonian effects are possible (40).

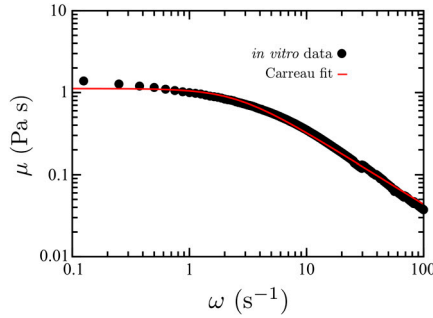


Fig. 4. Rheological study of the oocyte cytoplasm. Viscosity (in black) of the cytoplasm as a function of frequency ω . Red line is a fit of a Carreau model, $\mu = \mu_0(1 + (\lambda\omega)^2)^{n/2}$, with $n \approx 0.12$. The zero shear rate viscosity from the fit, $\mu_0 = 1.12$ Pa·s, slightly underestimates the observed value of 1.38 Pa·s, but this form accurately captures the characteristic time $\lambda = 0.4$ s.

At the shear rates measured by PIV ($\mathcal{O}(10^{-2})\text{s}^{-1}$) the cytoplasm is Newtonian and the viscous power per unit volume is $\Phi_v = 2\mu e_{ij}e_{ij}$, where $e_{ij} = (1/2)(\partial u_i/\partial x_j + \partial u_j/\partial x_i)$ is the rate of strain tensor measuring flow gradients (41), whose components are calculated directly from PIV data. This quantity represents a lower bound on the power per unit volume. A heuristic upper estimate on the power per unit volume, Φ_D , comes from dissipation at the scale of the mesh (see *SI Text*) where one considers the porous medium effects. Calculating the volume of the oocyte as a half ellipsoid, we determine total power, P_v and P_D , which bound the true power: $P_v < P_s < P_D$. For WT cells we find $3.2 \times 10^5 k_B T/s < P_s < 1.2 \times 10^6 k_B T/s$, and thus the number of motors contributing to streaming is $2.1 \times 10^3 < N_m < 8 \times 10^4$. Kinesins moving along microtubules can produce large scale effects on the surrounding cytoplasm, due to hydrodynamic coupling between motors (42). Therefore few motors could be capable of moving a large amount of fluid. Because only the lower bound is formal we will only consider the relative fractional changes to P_v to fractional changes in motor number and power. In *pat1* and *klc* mutants we see a reduction in P_v to $2.7 \times 10^5 k_B T/s$ and $2.6 \times 10^5 k_B T/s$, respectively. Based on the *Pat1* function it is plausible that the number of active motors in *klc* and *pat1* mutants is similar to WT, but with reduced motility. The lower bound estimates of streaming power in these mutants are reduced by 20% which, if the number of active motors is constant, implies the motor speed is reduced by 20%, again in striking agreement with in vitro data (28). This reduction further supports the relation between motor activity and flows, and strongly suggests that the work done by motor motion is dissipated by viscous mechanisms.

To study how streaming is affected by motor number, we analyzed oocytes that only express the constitutively active Khc Δ I Δ K, a Khc lacking the auto-inhibitory domain IAK. The IAK domain binds the motor domain, maintaining Khc in a folded, nonmotile state (43–45). If the IAK domain is mutated, then Khc is constitutively active, so the number of active motors doing work on the fluid in Khc Δ I Δ K oocytes is expected to be higher than in the control. We found in these Khc Δ I Δ K oocytes $\bar{u} = 30.03 \pm 1.8$ nm/s ($n = 6$), 1.5 times higher than in the WT, while the correlation length is unchanged. The lower bound estimate $P_v = 8.9 \times 10^5 k_B T/s$ is nearly 2.8 times that found in WT oocytes. If we assume that the speed of Khc Δ I Δ K is the same as Khc, we deduce 2.8 times as many motors are contributing to streaming in Khc Δ I Δ K oocytes as compared to WT. The expression of a full length Khc did not result in faster flows.

Kinesin drives streaming at mid-oogenesis and also transports *oskar* mRNA to the posterior. It has been proposed that this transport is a biased random walk (46); the long-ranged correlations we have found in the MT network motivate a biased *correlated* random walk model. To describe transport of such cargo we use the advection-diffusion equation

$$\frac{\partial c}{\partial t} + \nabla \cdot (\mathbf{u}c) = \nabla \cdot (\sigma \nabla c), \quad [2]$$

for the cargo concentration c , where $\mathbf{u}(\mathbf{x})$ is the coarse-grained local mean velocity on the network, averaged over a region much smaller than the oocyte size, centered at \mathbf{x} , and σ is the local velocity variance. The advection contribution $\nabla \cdot (\mathbf{u}c)$ describes motion of a parcel of *oskar* mRNA moving in the direction \mathbf{u} without spreading, while the effective diffusion term $\nabla \cdot (\sigma \nabla c)$ results from the random walk of the motors, and describes spreading of *oskar* mRNA. Estimates of \mathbf{u} and σ are (47) $\mathbf{u} = u_k \mathbf{t}$ and $\sigma = u_k^2 \tau$, where u_k is the typical Kinesin speed, τ is the mean run time, and \mathbf{t} is the mean orientation of the MTs on the coarse-graining scale.

One of the critical issues in transport in the oocyte is the effect of long-ranged correlations. Viewing fluctuations in the local network direction as noise in the local mean velocity \mathbf{u} , we separate \mathbf{u} into a bias vector, the moving average of the local velocity $\hat{\boldsymbol{\mu}} = \langle \mathbf{u} \rangle$, and a correlated fluctuation field $\mathbf{v} = \mathbf{u} - \hat{\boldsymbol{\mu}}$, the deviation from the moving average. The advective contribution to transport splits into two terms, and if we rescale by $\mathbf{x} \rightarrow \hat{\mathbf{x}} = \mathbf{x}/L$, $t \rightarrow s = tD/L^2$, $\boldsymbol{\mu} \rightarrow \hat{\boldsymbol{\mu}} = \boldsymbol{\mu}/|\boldsymbol{\mu}|$ and $\mathbf{v} \rightarrow \hat{\mathbf{v}} = \mathbf{v}/|\mathbf{v}|$ then Eq. 2 becomes

$$\frac{\partial c}{\partial s} + Pe_m \hat{\nabla} \cdot (\hat{\boldsymbol{\mu}}c) + Pe_f \hat{\nabla} \cdot (\hat{\mathbf{v}}c) = \hat{\nabla}^2 c, \quad [3]$$

where we have two Péclet numbers, $Pe_m = |\boldsymbol{\mu}|L/\sigma$ and $Pe_f = \sqrt{\langle \mathbf{v}^2 \rangle}L/\sigma$, where L is the size of the oocyte. Pe_m and Pe_f control the importance of the bias and correlated fluctuations respectively, and define the parameter space for transport in the oocyte. To estimate these Péclet numbers we assume the typical speed of the bias field is $|\boldsymbol{\mu}| = bu_k$ and $\sqrt{\langle \mathbf{v}^2 \rangle} = fu_k$, where b is the bias in the network, and f is the standard deviation of the orientation field. Then $Pe_m = bL/u_k\tau$ and $Pe_f = fL/u_k\tau$. These numbers contain information about the MT network (b and f) and the motor activity (u_k). Because the Péclet numbers depend inversely on the motor activity, increasing the motor run length ($u_k\tau$) decreases the effect of advection.

We propose a heuristic two-dimensional model of transport with a source (nurse cells) and a sink (posterior binding site) on opposite sides of a square region (Fig. 5A and B). To focus on the effects of correlations and bias in the microtubule network we adopt the simplified model of a perfectly absorbing sink, which holds literally if binding at the posterior is much faster than transport time scales. Using EB1 data (2) we find $b = 0.14$ and $f = 0.13$, and thus $Pe_m \sim Pe_f = 10$ –100 depending on motor activity. As mid-oogenesis lasts approximately 6 h, longer than any of the transport time scales, we consider the steady-state behavior, and in particular the flux of *oskar* mRNPs arriving at and bound to the posterior. Eq. 3 is solved numerically using commercial software (Comsol 4.2).

Consider first a spatially-uniform bias. In Fig. 5C we compare the flux vs. Pe_m (black) to the flux in the absence of fluctuations ($Pe_f = 0$) in red. Intuitively, for $Pe_m \gg Pe_f$ the flux collapses to the fluctuation-free result, but this occurs for surprisingly small values of the bias. In Fig. 5D we plot the fractional enhancement of the fluctuation field vs. Pe_f and $Pe_m/Pe_f\xi$, showing that if $Pe_m/Pe_f > \xi$, where $\xi = r_0/L$ is the dimensionless correlation length, then the fluctuation field does not significantly enhance transport. If we use the observed values from the streaming field, $\xi \sim 0.2$ and $Pe_m/Pe_f \sim 1$, then the fluctuation field should not be important. Because $J \propto Pe_m$ for large Pe_m we expect $J = u_k bc_o$, where c_o is the concentration at the source/nurse cell; the rate of *oskar* mRNA transport should increase linearly with motor activity and the strength b of the bias. Using the empirical values $b = 0.14$ and $u_k = 300$ nm/s (46), the typical time scale for localization of *oskar* mRNAs ($T = L/J/c_o$) would be approximately 32 min in this case of uniform bias.

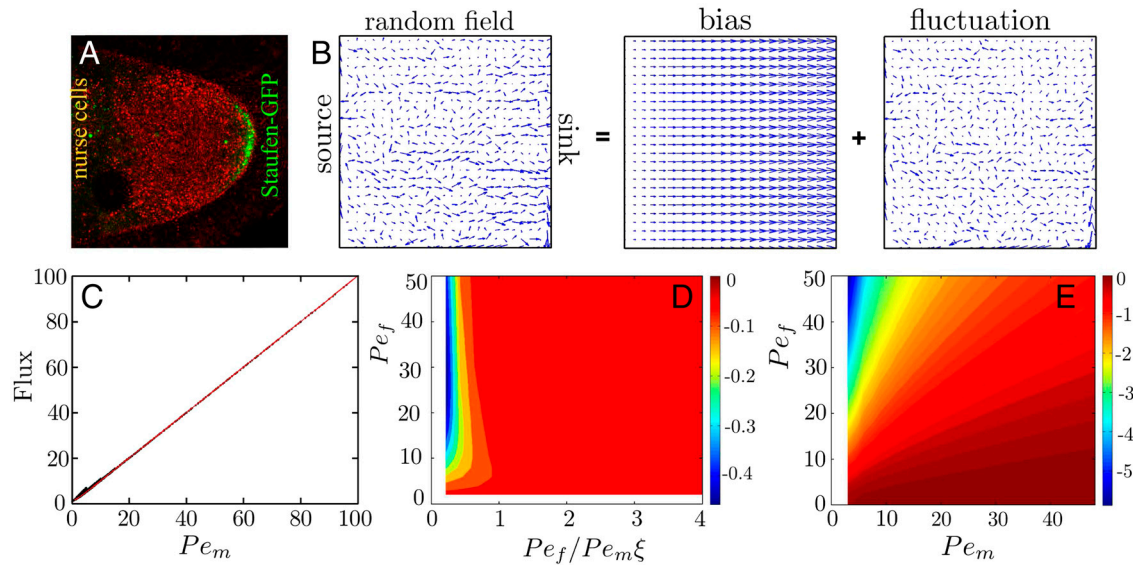


Fig. 5. Model and Results. The *Drosophila* oocyte (A, with Staufen-GFP in green, as a marker for *oskar* mRNA), is modeled as a square (B) with a source ($c(0, y, t) = c_0$), representing *oskar* mRNA entering the anterior from the nurse cells, and a sink ($c(L, y, t) = 0$), representing the posterior anchoring site. The other two boundaries are reflecting ($\partial_y c(x, 0, t) = \partial_y c(x, L, t) = 0$). Inside the square is a random biased correlated field to drive transport, which is partitioned into a bias field and the fluctuation field. (C) Flux for a uniform bias field. The steady state flux for a variety of correlation lengths, in black, plotted versus Péclet number Pe_m , in units of diffusive flux $J_D = J_o = u_k^2 \tau_c / L$. In red is the analytic solution without fluctuations, $J = -Pe_m((1 - e^{-Pe_m})^{-1} - 1)$, showing excellent agreement with the analytic solution for most parameter values. (D) The fractional deviation of the computational result from the analytic solution (black and red line respectively, in C). We note that computational solution is equal to or greater than the analytic solution. (E) Fractional deviation for a linear bias. We plot the fractional enhancement of the steady state flux with a fluctuations field. Without fluctuations the flux is $J = \sqrt{2Pe_m} / \pi / \text{erf}(\sqrt{Pe_m})$.

If the bias varies in space, as is known to be the case, the fluctuation field can be much more important and the flux at the boundary can be significantly modified. For simplicity, consider a linearly varying bias, $\hat{\mu} = \hat{x}/2$. In Fig. 5E we plot the fractional enhancement of the flux due to fluctuations for $\xi = 0.2$. For values like those found in the oocyte, we find the flux with a bias is at least twice that predicted by the bias alone. Therefore the fluctuation field should have a significant effect on the rate of mRNA localization at the posterior. Taking $Pe_f = Pe_m = 15$, $u_k = 300$ nm/s and a motor run length of $1 \mu\text{m}$, the time scale for mRNA localization is approximately 66 min, compared to approximately 133 min without the fluctuation field. The key mechanism for this effect is that fluctuations allow an mRNA to reach a region of higher bias faster than it would otherwise. Thus, long-ranged correlations significantly enhance the transport of *oskar* in the oocyte. Interestingly the speed of streaming, about 20 nm/s is comparable to the magnitude of the fluctuation field, $f_{u_k} \sim 20$ nm/s. As we have shown that streaming speeds depend directly on motor activity this relationship should hold for a variety of mutations, so one can consider that the streaming field has the same connection with transport as the MT architecture.

Conclusions

The quantification of cytoplasmic streaming we have outlined relates for the first time cellular changes affecting Kinesin activity and the large-scale properties of flows. Our finding of a relation between motor activity and cytoplasmic streaming holds not only for mid-oogenesis (stage 9), but also for the fast unidirectional movement of the ooplasm at later stages, as we also observe that flows at stage 11 are slower in *pat1* mutants than in WT flies. Our results also show that the local velocity of streaming is a functional of the MT concentration, MT orientation, and the density of active Kinesin.

One presumed function of streaming is facilitating the distribution of cytoplasmic components that do not diffuse fast enough for proper cellular activity. In *Drosophila* oocytes, flows are not essential for localization of *nanos* mRNA at late-oogenesis, but they enhance its translocation to the oocyte posterior (8). Similarly, streaming at mid-oogenesis is not essential for the localization

of *oskar* mRNA (7). However, our data suggest that motor-dependent flows could facilitate the localization of molecules by aiding the movement in the right direction of the cargo or cargo/motor complexes that detach from the MT cytoskeleton. The fact that streaming may be an essential variable when considering transport may be relevant to a range of process occurring in cells. The model framework introduced here allows for a quantitative understanding of the time scales of motor driven transport, and its structure is applicable to any system with motor driven transport.

Our findings of correlations between cytoplasmic streaming features and MT network architecture may allow the noninvasive, straightforward detection of streaming to be used to predict changes in cytoskeleton organization in vivo. This correlation is particularly interesting regarding tumorigenesis, where changes to the cytoskeleton occur (48), and quantified cytoplasmic streaming may thus serve as a diagnostic tool.

Materials and Methods

Live Imaging. Females were fattened on yeast for 16–24 h at 25°C. Ovaries were dissected in 10S Voltalef oil (Altechem) and examined under a 40x/1.3 Oil DIC Plan-Neofluar objective using a Leica LSM inverted confocal microscope. Auto-fluorescent vesicles were observed by reflection from the 561 nm laser line at stage 9 of oogenesis. **Movies S1** and **S2** were 200–500 frames long with a scan speed of 200 Hz (1 frame every 5.179 seconds). For simultaneous imaging of both microtubules and auto-fluorescent vesicles oocytes expressing JupiterGFP or TauGFP were examined as above, but using both 488 nm and 561 nm laser lines and a 100x/1.4 NA Plan-Apochromat.

Particle Image Velocimetry. PIV was performed with commercial software (FlowManager, Dantec Dynamics). An interrogation window of 16×16 pixels ($3 \times 3 \mu\text{m}$) with a 25% overlap was chosen, as this was much smaller than typical observed gradients in the flow. Any point that lies outside the cell was not considered. Probability distributions of speeds were generated by taking histograms of speeds for every oocyte, and then normalizing. Each of the normalized histograms was then averaged to generate the total probability function (Fig. 2A). Correlation functions were calculated using the simple vector vector correlation function (Eq. 1). For each PIV frame a correlation function was calculated, and these were then averaged to generate the correlation functions for each oocyte. The average across all oocytes is displayed in Fig. 3A. For correlations from EB1 microtubule tracks, we took track data from (2), kindly provided by R. Parton, I. Davis, and R.S. Hamilton, and



took the mean vector in $3 \mu\text{m}^2$ boxes, to provide a vector field similar to those found by PIV. Correlation functions were calculated on this coarse-grained field as before.

Drosophila Stocks, Microrheology, Transgenic Methods, MT Staining, and Germ-line Clones. See *SI Text* for details.

1. Kugler JM, Lasko P (2009) Localization, anchoring and translational control of oskar, gurken, bicoid and nanos mRNA during drosophila oogenesis. *Fly (Austin)* 3:15–28.
2. Parton RM, et al. (2011) A PAR-1-dependent orientation gradient of dynamic microtubules directs posterior cargo transport in the *Drosophila* oocyte. *J Cell Biol* 194:121–135.
3. Gutzzeit H, Koppa R (1982) Time-lapse film analysis of cytoplasmic streaming during late oogenesis of *Drosophila*. *J Embryol Exp Morphol* 67:101–111.
4. Theurkauf W, Smiley S, Wong M, Alberts B (1992) Reorganization of the cytoskeleton during *Drosophila* oogenesis—implications for axis specification and intercellular transport. *Development* 115:923–936.
5. Theurkauf WE (1994) Premature microtubule-dependent cytoplasmic streaming in cappuccino and spire mutant oocytes. *Science* 265:2093–2096.
6. Palacios IM, Johnston DS (2002) Kinesin light chain-independent function of the Kinesin Heavy Chain in cytoplasmic streaming and posterior localisation in the *Drosophila* oocyte. *Development* 129:5473–5485.
7. Serbus LR, Cha BJ, Theurkauf WE, Saxton WM (2005) Dynein and the actin cytoskeleton control kinesin-driven cytoplasmic streaming in drosophila oocytes. *Development* 132:3743–3752.
8. Forrest KM, Gavis ER (2003) Live imaging of endogenous mRNA reveals a diffusion and entrapment mechanism for nanos mRNA localization in *Drosophila*. *Curr Biol* 13:1159–68.
9. Corti B (1774) *Osservazione Microscopiche sulla Tremella e sulla Circolazione del Fluido in Una Planto Acquaguala* (Appresso Giuseppe Rocchi, Lucca, Italy).
10. Shimmen T, Yokota E (2004) Cytoplasmic streaming in plants. *Curr Opin Cell Biol* 16:68–72.
11. Pickard WF (1974) Hydrodynamic aspects of protoplasmic streaming in Chara braunii. *Protoplasma* 82:321–339.
12. Allen NS, Allen RD (1978) Cytoplasmic streaming in green plants. *Ann Rev Biophys Bioeng* 7:497–526.
13. Verchot-Lubicz J, Goldstein RE (2010) Cytoplasmic streaming enables the distribution of molecules and vesicles in large plant cells. *Protoplasma* 240:99–107.
14. Pickard WF (2003) The role of cytoplasmic streaming in symplastic transport. *Plant Cell Environ* 26:1–5.
15. Goldstein RE, Tuval I, van de Meent JW (2008) Microfluidics of cytoplasmic streaming and its implications for intracellular transport. *Proc Natl Acad Sci USA* 105:3663–3667.
16. van de Meent JW, Tuval I, Goldstein RE (2008) Nature's microfluidic transporter: Rotational cytoplasmic streaming at high Péclet numbers. *Phys Rev Lett* 101:178102.
17. Hochachka PW (1999) The metabolic implications of intracellular circulation. *Proc Natl Acad Sci USA* 96:12233–12239.
18. Hecht I, Rappel WJ, Levine H (2009) Determining the scale of the bicoid morphogen gradient. *Proc Natl Acad Sci USA* 106:1710–1715.
19. Yi K, et al. (2011) Dynamic maintenance of asymmetric meiotic spindle position through Arp2/3-complex-driven cytoplasmic streaming in mouse oocytes. *Nat Cell Biol* 13:1252–1258.
20. Ajduk A, et al. (2011) Rhythmic actomyosin-driven contractions induced by sperm entry predict mammalian embryo viability. *Nat Commun* 2:417.
21. Nothnagel EA, Webb WW (1982) Hydrodynamic models of viscous coupling between motile myosin and endoplasm in Characean algae. *J Cell Biol* 94:444–454.
22. Shimmen T (2007) The sliding theory of cytoplasmic streaming: fifty years of progress. *J Plant Res* 120:31–43.
23. Yamamoto K, et al. (2006) Chara myosin and the energy of cytoplasmic streaming. *Plant Cell Physiol* 47:1427–1431.
24. Wolff K, Marenduzzo D, Cates ME (2012) Cytoplasmic streaming in plant cells: the role of wall slip. *J R Soc Interface* 9:1398–1408.
25. Adrian RJ (1991) Particle-imaging techniques for experimental fluid mechanics. *Ann Rev Fluid Mech* 23:261–304.
26. Willert C, Gharib M (1991) Digital particle image velocimetry. *Exp Fluids* 10:181–193.
27. Drescher K, Goldstein RE, Michel N, Polin M, Tuval I (2010) Direct measurement of the flow field around swimming microorganisms. *Phys Rev Lett* 105:168101.
28. Loiseau P, Davies T, Williams LS, Mishima M, Palacios IM (2010) *Drosophila* pat1 is required for Kinesin-1 to transport cargo and to maximize its motility. *Development* 137:2763–2772.
29. Gonzalez-Reyes A, Elliott H, Johnston D, St (1995) Polarization of both major body axes in *Drosophila* by gurken-torpedo signaling. *Nature* 375:654–658.
30. Roth S, Neuman-Silberberg FS, Barcelo G, Schupbach T (1995) Cornichon and the EGF receptor signaling process are necessary for both anterior-posterior and dorsal-ventral pattern formation in *Drosophila*. *Cell* 81:967–978.
31. Dombrowski C, Cisneros L, Chatkaew S, Kessler JO, Goldstein RE (2004) Self-concentration and large-scale coherence in bacterial dynamics. *Phys Rev Lett* 93:098103.
32. Micklem DR, et al. (1997) The mago nashi gene is required for the polarisation of the oocyte and the formation of perpendicular axes in *Drosophila*. *Curr Biol* 7:468–478.
33. Karpova N, Bobinac Y, Fouix S, Huitorel P, Debec A (2006) Jupiter, a new *Drosophila* protein associated with microtubules. *Cell Motil. Cytoskeleton* 63:301–312.
34. Purcell E (1977) Life at low Reynolds number. *Am J Phys* 45:3–11.
35. Svoboda K, Block S (1994) Force and velocity measured for single kinesin molecules. *Cell* 77:773–784.
36. Mofrad MRK (2009) Rheology of the cytoskeleton. *Annu Rev Fluid Mech* 41:433–453.
37. Mason TG, Ganesan K, van Zanten JH, Wirtz D, Kuo SC (1997) Particle tracking microrheology of complex fluids. *Phys Rev Lett* 79:3281–3285.
38. Xu J, Viasnoff V, Wirtz D (1998) Compliance of actin filament networks measured by particle-tracking microrheology and diffusing wave spectroscopy. *Rheol Acta* 37:387–398.
39. Bausch AR, Möller W, Sackmann E (1999) Measurement of local viscoelasticity and forces in living cells by magnetic tweezers. *Biophys J* 76:573–579.
40. Holzwarth G, Bonin K, Hill DB (2002) Forces required of kinesin during processive transport through cytoplasm. *Biophys J* 82:1784–90.
41. Batchelor G (2000) *An Introduction to Fluid Dynamics* (Cambridge Univ Press, Cambridge, UK).
42. Deutsch JM, Brunner ME, Saxton WM (2011) The mechanics of a microscopic mixer: microtubules and cytoplasmic streaming in *Drosophila* oocytes. arXiv:1101.2225.
43. Hackney DD (1995) Highly processive microtubule-stimulated APT hydrolysis by dimeric kinesin head domains. *Nature* 377:448–450.
44. Hackney DD, Stock MF (2000) Kinesin's IAK tail domain inhibits initial microtubule-stimulated ADP release. *Nat Cell Biol* 2:257–260.
45. Kaan HYK, Hackney DD, Kozielski F (2011) The structure of the kinesin-1 motor-tail complex reveals the mechanism of autoinhibition. *Science* 333:883–885.
46. Zimyanin VL, et al. (2008) In vivo imaging of oskar mRNA transport reveals the mechanism of posterior localization. *Cell* 134:843–853.
47. Berg HC (1993) *Random Walks in Biology* (Princeton Univ Press, Princeton, New Jersey).
48. Suresh S (2007) Biomechanics and biophysics of cancer cells. *Acta Biomater* 3:413–438.